

# **The bilayer collective properties govern the interaction of an HIV-1 antibody with the viral membrane**

**Running title:** HIV antibody interaction with the membrane

P. Carravilla, L. Darre, I.R. Oar-Arteta, A. G. Vesga, E. Rujas, G. de las Heras-Martínez, C. Domene, J.L. Nieva<sup>\*</sup>, J. Requejo-Isidro<sup>\*</sup>

<sup>\*</sup>To whom correspondence should be addressed: Prof. J.L. Nieva, & Dr J. Requejo-Isidro

**Keywords:** lipid-protein interaction, MPER, antibody, quantitative fluorescence microscopy, protein diffusion, HIV neutralisation

## **Abstract**

Efficient engagement with the envelope glycoprotein (Env) membrane-proximal external region (MPER), results in robust blocking of viral infection by a class of broadly neutralising antibodies (bnAbs) against HIV. Developing an accommodation surface that engages with the viral lipid envelope appears to correlate with the neutralising potency displayed by these bnAbs. The nature of the interactions established between the antibody and the lipid is nonetheless a matter of debate, with some authors arguing that anti-MPER specificity arise only under pathological conditions in autoantibodies endowed with stereospecific binding sites for phospholipids. However, bnAb-lipid interactions are often studied in systems that do not fully preserve the biophysical properties of lipid bilayers, and therefore questions on binding specificity and the effect of collective membrane properties in the interaction are still open. Here, to evaluate the specificity of lipid interactions of an anti-MPER bnAb (4E10) in an intact membrane context, we determine quantitatively its association with lipid bilayers by means of scanning fluorescence correlation spectroscopy and all-atom molecular dynamic simulations. Our data support that 4E10 establishes electrostatic and hydrophobic interactions with the viral membrane surface, and that the collective physical properties of the lipid bilayer influence 4E10 dynamics therein. We conclude that establishment of peripheral, non-specific electrostatic interactions with the viral membrane through accommodation surfaces may assist high-affinity binding of HIV-1 MPER epitope at membrane interfaces. These findings highlight the importance of considering antibody-lipid interactions in the design of antibody-based anti-HIV strategies.

## **Statement of significance**

The viral membrane plays a crucial role in HIV neutralisation by many anti-MPER antibodies. [Understanding the mechanistics of membrane-antibody interaction is key to engineering anti-MPER based vaccines.](#)

We describe the interaction of the anti-HIV-1 broadly neutralising antibody 4E10 with a membrane, correlating membrane-antibody association with the bilayer collective properties. To do so, we have applied, for the first time to our knowledge, a methodology based on measuring antibody diffusion at the bilayer to describe the nature (hydrophobic, electrostatic or lipid-specific) of the antibody-membrane association.

Our findings are important to understand the membrane-mediated events leading to HIV-1 neutralisation by anti-MPER antibodies. Besides, the methodology we have used will contribute to describing the mechanistic basis of antibody-epitope recognition in a membrane context.

## **Introduction**

The human immunodeficiency virus (HIV) deploys several strategies to evade immune neutralisation. Among them, the rapid sequence variation of the envelope glycoprotein (Env) with successive replication cycles facilitates escape from the adaptive immune response. Access to antibodies (Abs) is hindered further due to the scarce number of copies of this protein present on the virion surface (1). Anti-HIV broadly neutralising antibodies (bnAbs) are capable of neutralising genetically diverse HIV strains usually targeting conserved regions of the Env protein, the only viral protein found on the outside of the virus (1).

Among all known bnAbs, those with the largest breadth (such as 4E10 and 10E8) bind to a highly conserved region close to the transmembrane domain of the gp41 Env subunit, termed membrane proximal external region (MPER) (1, 2) (Fig. 1A). MPER is responsible for the disruption of the HIV membrane during fusion of the cell plasma membrane and the viral envelope (3-5).

Another peculiarity of anti-MPER bnAbs is their functional association with the viral membrane: epitope binding occurs at the interface of the viral lipid envelope and relies on antibody-lipid interactions (6). Mutation of lipid-interacting residues prevents Env binding and

subsequent viral neutralisation (6-9). This idea was further supported by the recently resolved crystal structure of the anti-MPER bnAbs 4E10 and 10E8 in complex with lipids, revealing a surface where interactions between backbone atoms of the protein and glycerol groups, phosphate moieties and upper section of the lipid tails of phospholipids can be observed (10, 11).

This functional and structural evidence stress the need for understanding the mechanisms governing the dynamic Ab-lipid binding process at the membrane interface. Despite the vast available knowledge on the molecular basis governing Ab-epitope recognition, little is known on the contribution of membrane interactions to this phenomenon in some relevant instances, such as bnAbs against HIV MPER.

In this work, we focused on the interaction of 4E10, a well-characterised pan-neutralising anti-MPER bnAb. 4E10-membrane interaction is thought to occur through the concerted interplay of (i) an electrostatic attraction between the membrane-associated paratope area (MAPA) (Fig. 1A, bottom view) and the lipid polar heads (7, 12) and (ii) a deeper hydrophobic interaction between the anti-MPER Ab heavy-chain complementary determining region 3 (HCDR3) and the lipid bilayer (Fig. 1A) (10, 13). In that regard, 4E10 resembles the features of peripheral membrane proteins (7).

To quantitatively interrogate the nature of 4E10 interaction with the membrane we correlated the diffusional behaviour of the 4E10 Fab on controlled model-membrane systems with their biophysical properties, such as surface membrane potential and lipid-packing. To do so, we used scanning fluorescence correlation spectroscopy (sFCS) to accurately measure diffusion coefficients at the surface of a membrane (14, 15), as well as two-photon generalised polarisation imaging to quantify the membrane lipid-packing (16, 17). In addition, molecular dynamics (MD) simulations with a total accumulated time of 1  $\mu$ s were used to obtain atomic-

level insights on the interaction of 4E10 with the bilayer, complementing the experimental results.

Our quantitative findings support that 4E10 dynamics on virus-like lipid membranes are governed by [collective biophysical properties, such as surface membrane](#) potential and molecular order, and argue against a specific docking interaction between 4E10 and PS (phosphatidylserine) (Fig. 1B), the most abundant anionic lipid in the viral membrane (18). The three known 4E10-virus interaction sites (MPER specificity pocket, HCDR3 and MAPA) condition the diffusion of 4E10 Fab on virus-like membranes, suggesting that these interactions overall contribute to the formation and stability of the 4E10-HIV complex. Thus, we hypothesise that 4E10-membrane interaction sites evolved to increase affinity for its primary epitope MPER through the formation of secondary Ab-lipid interactions. These observations are key to the successful engineering of MPER-targeting immunogens, as well as to defining the structural components that must be preserved when developing antibodies as immunotherapeutic agents.

## Materials and Methods

### Lipids and MPER

1,2-dioleoylphosphatidylcholine (DOPC), 1,2-dioleoylphosphatidylserine (DOPS), cholesterol (Chol) and egg sphingomyelin (eSM, containing  $\approx$  86% N-palmitoyl SM) were purchased from Avanti Polar Lipids (Birmingham, AL, USA). 6-dodecanoyl-2-dimethylaminonaphthalene (Laurdan) was obtained from Molecular Probes (Eugene, OR, USA). Fluorescently labelled 1,2-dioleoylphosphatidylethanolamine (DOPE-STAR RED) was purchased from Abberior (Abberior GmbH, Göttingen, Germany). Phospholipid stock concentrations were determined by phosphate assay. The MPER peptide (KKDKWASLWNWFDITNWLWYIKLFIMIVGKKK) was synthesized in C-terminal carboxamide form by solid-phase methods using Fmoc chemistry, purified by reverse-phase high-performance liquid chromatography (HPLC), and characterized by matrix-assisted laser desorption ionization–time-of-flight (MALDI-TOF) mass spectrometry (purity > 95%).

#### **4E10 Fab purification and labelling**

The 4E10 Fab sequence was cloned in pColaDuet plasmid and expressed in *Escherichia coli* T7-shuffle strain. Recombinant expression was induced at 18°C overnight with 0.4 mM isopropyl-D-thiogalactopyranoside when the culture reached an optical density of 0.8. Cells were harvested and centrifuged at 8000 ×g, after which they were resuspended in a buffer containing 50 mM HEPES (pH 7.5), 500 mM NaCl, 35 mM imidazole, DNase (Sigma-Aldrich, St. Louis, MO) and an EDTA-free protease inhibitor mixture (Roche, Spain). Cell lysis was performed using an Avestin Emulsiflex C5 homogenizer. Cell debris was removed by centrifugation, and the supernatant loaded onto a nickel-nitrilotriacetic acid (Ni-NTA) affinity column (GE Healthcare). Elution was performed with 500 mM imidazole, and the fractions containing the His-tagged proteins were pooled, concentrated and dialysed against 50 mM sodium phosphate (pH 8.0), 300 mM NaCl, 1 mM DTT, and 0.3 mM EDTA in the presence of purified protease Tobacco etch virus (TEV). Fabs were separated from the TEV and cleaved peptides containing the His6× tag by an additional step in a Ni-NTA column. The flow-through fraction containing the Ab was dialysed overnight at 4 °C against sodium acetate (pH 5.6) supplemented with 10% glycerol and subsequently loaded onto a MonoS ion exchange chromatography (IEC) column (GE Healthcare). Elution was carried out with a gradient of potassium chloride and the fractions containing the purified Fab concentrated and dialysed against a buffer containing 10 mM sodium phosphate (pH 7.5), 150 mM NaCl, and 10% glycerol. For the preparation of the Δloop mutant Fab (W100-G100a-W100b-L100c residues substituted by an S-G dipeptide), the KOD-Plus mutagenesis kit (Toyobo, Osaka, Japan) was employed following the instructions of the manufacturer. Fab labelling was attained by introducing first titratable Cys residues at position Cys228HC of the 4E10 sequence, and then by modifying those with a sulfhydryl-specific iodacetamide derivative of the Abberior STAR RED (KK114) probe (Abberior GmbH, Göttingen, Germany). After purification, fluorescence emission measured after SDS-PAGE and absorbance measurements confirmed almost total titration of the single free Cys residues in the Fabs.

## Preparation of Giant Unilamellar Vesicles

Giant unilamellar vesicles (GUVs) were produced by spontaneous swelling following the procedures described in (17, 19). For preparation of MPERb-containing GUVs, vesicles and peptides were mixed at 1:1000 peptide:lipid molar ratio for 15 minutes (25 °C) prior to incubation with silica bead. Dried silica beads covered with lipid-peptide mixtures were collected and transferred to an 85 g/L sucrose buffer to induce spontaneous swelling of GUVs. Formed vesicles were transferred to a bovine serum albumin (BSA)-blocked observation dish in an isosmotic 10 mM HEPES, 150 mM KCl (pH 7.4) buffer that already included 4E10 Fab to a final concentration of 3-20 nM for sFCS experiments and 200 nM for imaging experiments. GUVs and Abs were incubated for 15 minutes and subsequently imaged.

Atto 647-labelled Annexin A5 was purchased from Adipogen (Liestal, Switzerland). For the Annexin A5 experiments, GUVs were incubated with this protein in a 2 mM CaCl<sub>2</sub> - HBS buffer.

## Imaging lipid packing at the membrane: Generalised Polarisation (GP)

Lipid-packing imaging and quantification through the ratiometric quantity generalised polarisation (GP) (20) was performed as previously described in detail (16, 17). Briefly, images were acquired on a Leica TCS SP5 II microscope (Leica Microsystems GmbH, Wetzlar, Germany). Laurdan-stained GUVs (1:100 mole fraction) were excited at 780 nm using a ×63 water-immersion objective (numerical aperture, NA=1.2) and 512x512-pixel images. The fluorescence emission was simultaneously imaged at 435 ± 20 nm and at 500 ± 10 nm. GP images were computed for every pixel in the image (equation 1), where  $I_B$  is the intensity in the blue channel, and  $I_R$  the intensity in the green channel:

$$GP = \frac{I_B - G \times I_R}{I_B + G \times I_R} \quad (1)$$

The  $G$  factor accounts for the relative sensitivity of the two channels, calibrated using a 5 µM Laurdan solution in pure DMSO ( $GP_{cal}=0.207$  at 22 °C) (21):

$$G = \frac{GP_{cal} + GP_{cal} \times GP_{obs} - 1 - GP_{obs}}{GP_{obs} + GP_{cal} \times GP_{obs} - 1 - GP_{cal}} \quad (2)$$

where  $GP_{obs}$  is the GP value determined for the standard Laurdan-DMSO solution before calibration ( $G=1$ ).

The uncertainty of the GP values in the text is given by the experiment SEM (standard error of the mean); whiskers in the GP box-and-whiskers plot span to  $\pm 1.5$  times SD (standard deviation).

### **Diffusion at the membrane: Scanning Fluorescence Correlation Spectroscopy (sFCS)**

Scanning Fluorescence Correlation Spectroscopy (sFCS) was used to study the diffusional behaviour and intermolecular interactions of fluorescently labelled proteins bound to giant unilamellar vesicles (Fig. S1). Excitation and detection was performed through a water immersion objective HCX PL APO 63x/1.20 W CORR Lbd BI (Leica) on a confocal Leica SP5 using the Avalanche Photodiodes (APD) (Excelitas Technologies SPCM-AQRH-W3) fitted on the microscope DD X1 port. Abberior STAR RED (Abberior GmbH, Göttingen) tagged Fabs were excited at 633 nm and the fluorescent emission was detected through a BP647-703 nm filter. The average power density at the sample plane was 50 kW/cm<sup>2</sup>. Photon arrival times were recorded using a SPC830 TCSPC card (Becker & Hickl, Berlin), which also registered the pixel, line and frame signals from the scanner in order to track the beam position at the sample. An HRT-82 Eight Channel Router (Becker & Hickl) for the APDs was used to spectrally tag the APD output for the SPC830. The whole system was externally clocked at 20 MHz.

The imaging mode at the microscope was set to *xt* (line-scanning) at 1400 Hz scanning frequency and the SPC830 detection mode was set to FIFO image. The scanning length spanned over 16.64  $\mu$ m, binned in 64 pixels of 260 nm each. GUV membranes were scanned for 90-120 s. The SPC830 binary output files were decoded using an in-house developed Matlab routine. The *xt* photon trace was corrected for the vesicle drift and subsequently autocorrelated with a



minimal lag-time fixed by the inverse of the scanning frequency. The resulting curve  $G(\tau)$  was finally fit to a 2D diffusion model:

$$G(\tau) = \frac{1}{N} \left(1 + \frac{\tau}{\tau_D}\right)^{-1/2} \left(1 + \frac{\tau}{S^2 \tau_D}\right)^{-1/2} \quad (3)$$

where  $\tau$  is the lag-time,  $\tau_D$  the diffusion time,  $N$  the average number of molecules in the focal volume and  $S$  ratio of the axial ( $z_o$ ) to the radial ( $\omega_o$ )  $1/e^2$  dimensions of the confocal volume.  $\omega_o$  and  $z_o$  were obtained after calibrating the volume using dyes with known diffusion (Alexa 633,  $D=305\mu\text{m}^2/\text{s}$  in HEPES buffer at  $21^\circ\text{C}$ ). Finally, the diffusion coefficient is  $D= \omega_o^2 / (4 \tau_D)$ .

Determination of the average diffusion coefficient and experiment SD for every sample and membrane composition comprised at least 3 independent experiments and more than 9 measurements (typically 19 measurements per experiment). The shortest time lag for the calculation of the autocorrelation function in sFCS experiments is fixed by the excitation beam scanning frequency, hindering the observation of autocorrelation characteristics at shorter time lags. This, in turn, may affect the uncertainty of the fitted parameters. To ensure the reliability of the fitted parameters we analysed the uncertainty due to the fitting procedure and that given by the overall experimental variability (experiment SD). Support plane analysis of the diffusion coefficient  $\chi_R^2$  surface (22) (Fig. S2) typically showed a steep minimum at the value of  $D$  that minimised  $\chi_R^2$  and a fitting uncertainty at the 68% confidence level that was always smaller than the experiment SD. This indicated that variability in sample preparation and related experimental procedures, rather than fitting, was the main source of uncertainty, thus guaranteeing the reliability of the retrieved parameters.

The uncertainty of the diffusion coefficients given in the text is given by the experiment SEM unless otherwise stated; whiskers in the box-and-whiskers plots span to  $\pm 1.5$  times SD. Autocorrelation curves shown in Figs. 2, 3 and 4 were normalised after fitting to allow easier visual comparison between samples with different  $D$ . All in-house developed software tools are available upon request.

### Estimation of molecular mean area and membrane surface potential

The surface potential ( $\psi_s$ ) of a charged membrane immersed in a monovalent electrolyte bath where only one species of ions in solution neutralizing the charged surface is considered, is (23):

$$\psi_s = -\frac{4K_B T}{e} \arctan \left( -\frac{b}{\lambda_D} + \sqrt{\left(\frac{b}{\lambda_D}\right)^2 + 1} \right) \quad (4)$$

where  $K_B$  is the Boltzmann constant,  $T$  the temperature,  $e$  the electron charge,  $b = e (2\pi\lambda_B |\sigma|)^{-1}$ , with  $\lambda_B$  the Bjerrum length,  $\sigma$  the surface charge-density, and  $\lambda_D$  the Debye-Hückel screening length ( $\lambda_D = 0.304 n_0^{-0.5}$  in nm where  $n_0$  is the electrolyte strength in Molar units).

The surface potential of the DOPS:Chol:DOPC membranes was calculated using a  $60 \pm 1 \text{ \AA}^2$  mean molecular area of 18-carbon DOPS in 0.150 M NaCl solution at 300 K, determined by Molecular Dynamics simulations.

### Molecular modelling

The structure of the 4E10 Fab (chains H and L only) in the apo form were obtained from the crystal structure deposited with PDB ID 5CIP. A short missing loop in chain H (residues 128-135) was reconstructed using the homologous loop present in a holo form of the protein (PDB ID 2FX7). Residues protonation states were obtained using H++ at neutral pH (24-26). A DOPS:Chol:DOPC (0.45:0.35:0.20) lipid bilayer was generated using CHARMM-GUI (27-31). The protein was placed on the surface of the membrane oriented so that residues S74, S30 and G27 were close to the membrane surface (orthogonal distance between the bilayer head-groups and the geometric centres of S74, S30, and G27 at  $\approx 9 \text{ \AA}$ ). The system was centred in a simulation box of dimensions  $134 \times 135 \times 157 \text{ \AA}^3$ , solvated, and  $\text{Na}^+/\text{Cl}^-$  ions were added to neutralize the system and to achieve a bulk ionic concentration of 150mM. The CHARMM36m force field (32) was used to represent the protein, CHARMM36 (33) was used for the lipids, the TIP3P model (34) for

water, and the standard CHARMM and NBFIX parameters were used for ions (35, 36). The system was energy minimized in 5000 steps of geometry optimization, and equilibration at 300 K and 1.01325 bar was achieved in 1 ns of MD in the NpT-ensemble. Position restraints on the protein backbone atoms were applied during equilibration to maintain the initial structure. Semi-isotropic pressure coupling at 1.01325 bar was accomplished using the Nose-Hoover Langevin piston (37, 38) while temperature was maintained at 300 K by means of the Langevin thermostat (39). The particle mesh Ewald algorithm (40) with grid spacing of 1 Å was used for long-range electrostatic interactions and van der Waals forces were smoothly switched off between 10-12 Å. A Verlet neighbour list with pairlist distance of 16 Å was used. Equations of motions were integrated using the multi time step algorithm Verlet-I/r-RESPA (41). The RATTLE algorithm (42) was used to constrain bonds involving hydrogen atoms allowing for 2 fs time steps. Long-range electrostatic forces were updated every time step. Production MD simulations were carried out in two replicas, MD replica I (750 ns) and MD replica II (250 ns). The MD production run was carried out for 250 ns. All calculations were performed using the NAMD 2.10 software package (43).

## Results

### **Electrostatic and hydrophobic association to the viral membrane are essential for efficient epitope binding**

With the aim of understanding the role of Ab-membrane interactions in the 4E10-mediated neutralisation, we studied the 4E10 Fab behaviour on model giant unilamellar vesicles (GUVs) that were prepared from a five-lipid mixture derived from the HIV lipidome (virus-like mixture: PC:Chol:SM:PE:PS 14:46:17:16:7) (16, 18). To address the factors governing the interaction of 4E10 with membrane lipids, we included the unsaturated lipids [DOPC](#), [DOPE](#) and [DOPS](#) ([DO](#) denotes [dioleoyl](#)), which facilitate association of the Ab to the bare lipid bilayer (7, 8). We fluorescently tagged the 4E10 Fab with Abberior STAR RED and studied its binding and diffusive

behaviour on naked or MPER peptide-containing virus-like GUVs. Pure lipid GUVs constitute a controlled environment to study the membrane-dependent steps that contribute to epitope recognition, while MPER-loaded GUVs constitute an adequate model for Ab-epitope recognition in a lipid bilayer environment.

We first evaluated 4E10 binding to the virus-like GUVs using intensity-based confocal microscopy (Fig. 2A-B). 4E10 Fab readily partitioned virus-like vesicles that did not contain MPER (naked) (Fig. 2A). The reason can be ascribed to the electrostatic attraction between the Fab and the membrane and the interaction between the hydrophobic residues in the HCDR3 loop and the bilayer. As a negative control for this interaction we used another STAR RED-tagged bnAb, PGT145 (44). PGT145 is known to bind to the Env apex (farther apart from the viral membrane) and did not exhibit any partition to the membrane (Fig. 2C), confirming the non-random association of 4E10 to the membrane. To identify the contribution of each type of interaction, we independently prevented first, the hydrophobic contact of the Fab with the bilayer through the ablation of the hydrophobic residues at the HCDR3 loop tip (4E10  $\Delta$ loop), and second, the electrostatic attraction between 4E10 MAPA and the membrane removing the negatively charged PS lipids from the bilayer (0% PS, PC:Chol:SM:PE 17:46:17:20). In the absence of its epitope, 4E10 Fab binding to the naked GUVs was not observed in either case (Fig. 2A). Both types of interactions are, therefore, necessary for 4E10 Fab binding to the **naked** GUVs. When presented to MPER-loaded virus-like GUVs (Fig. 2B), vesicles appeared brighter because of the Ab affinity for the peptide. In contrast to naked vesicles, we found that deletion of the hydrophobic residues or removal of the charged lipids from the membrane only partially disrupted binding to the vesicles. Even the simultaneous arrest of both **electrostatic and hydrophobic** interactions did not totally prevent Ab binding to MPER (Fig. 2B).

A quantitative description of the molecular contact of 4E10 Fab with the bilayer was obtained through the study of the diffusional regime of the Fab on the membrane using sFCS (Fig. S1).

Point-FCS (pFCS) and sFCS are single-molecule sensitivity techniques that allow the diffusion coefficient of a molecule to be determined in solution (pFCS) or as the membrane-bound molecule diffuses on the surface of a vesicle (sFCS) (14, 15). The diffusion coefficient of the 4E10 Fab in the aqueous buffer was  $95 \pm 1 \mu\text{m}^2 \text{s}^{-1}$  (measured by pFCS), as expected given its molecular weight (47.8 kDa) (Fig. 2D). However, sFCS measurements revealed that the diffusion coefficient of the 4E10 Fab on the surface of naked virus-like vesicles decreased to  $8.3 \pm 0.5 \mu\text{m}^2 \text{s}^{-1}$  (Fig. 2D-E), caused by the slower dynamics of membrane lipid phases.

The molecular model for epitope recognition posits that the interaction of the Fab 4E10 heavy chain with membrane occurs through a surface patch with net positive charge (Fig 1A, see also MD simulations below). Consistent with this possibility the theoretical pI of the 4E10 heavy-chain is 9.34. To probe the effect of the electrostatic attraction, rather than removing the charged components, which would prevent Ab association, we increased the membrane net negative surface charge by increasing the anionic PS lipid concentration up to 37 mol % (Chol:SM:PS 46:17:37). This resulted in a significant decrease of the diffusion coefficient to  $5.0 \pm 0.4 \mu\text{m}^2 \text{s}^{-1}$ , further confirming the effect of the electrostatic contribution to the 4E10-membrane interaction (Fig. 2D-E).

We next addressed the effect of the membrane on 4E10 Fab binding to MPER. The Fab-epitope interaction could be restricted to the epitope binding site, that is, a binary interaction, or be mediated or modulated by the membrane through a ternary interaction. Compared to the naked GUVs, 4E10 Fab diffusion further decreased to  $2.6 \pm 0.2 \mu\text{m}^2 \text{s}^{-1}$  on MPER-loaded virus-like GUVs (Fig. 2D-E). Interestingly, the  $\Delta$ loop variant, which lacks the HCDR3 hydrophobic loop that inserts in the membrane showed a diffusion three times faster ( $7.2 \pm 0.8 \mu\text{m}^2 \text{s}^{-1}$ ) than the wild type Fab. This result demonstrated that 4E10 Fab dynamics are mainly governed by Ab-lipid interactions, since the wild type and  $\Delta$ loop versions of 4E10 Fab diffused differently upon epitope binding. Finally, the electrostatic interaction in the presence of MPER could not be

reliably probed due to the patchy distribution of the Fab on MPER containing GUVs made out of neutral lipids (Fig. 2B).

### **Membrane lipid packing governs 4E10 Fab diffusion**

Our results in the previous section support that 4E10-envelope interactions rely on the electrostatic attraction between the Ab residues and the negatively charged membrane together with the anchoring of the Ab HCDR3 loop hydrophobic groups in the bilayer. These results are consistent with previous reports (7, 45). We therefore set to evaluate systematically the contribution of collective biophysical properties of the bilayer, namely lipid packing and surface charge density, to 4E10 Fab interaction with membranes.

To this aim, we prepared PS:Chol:PC vesicles with increasing Chol content while keeping PS content constant (30%, estimated surface potential -68 mV). Adding Chol to a fluid bilayer rigidifies the membrane, resulting in increased lipid packing. To quantify membrane packing we used two-photon Generalised Polarisation (GP) imaging of Laurdan-stained GUVs. Laurdan is a hydrophobic polarity probe; when incorporated into a bilayer its fluorescence emission is a function of the hydration and viscosity of the membrane, reflecting its phase state (20). Laurdan fluorescence emission in loosely-packed membranes, which accommodate more interstitial water molecules, will be shifted to the red edge of the spectrum, while in tightly packed membranes, poorly hydrated, will be shifted to the blue. A wavelength-ratiometric parameter, termed Generalised Polarisation (20), quantifies Laurdan's spectral shift, providing an indirect measurement of membrane order through packing (16).

The effect of increasing Chol on 4E10 Fab diffusion on the membrane was to decrease the diffusion coefficient of the Fab from  $8.3 \pm 0.7 \mu\text{m}^2 \text{s}^{-1}$  for 20% Chol mixtures to about half this value ( $4.1 \pm 0.3 \mu\text{m}^2 \text{s}^{-1}$ ) when Chol content was increased to 50% (Fig. 3A-B). This reduction correlated with the increase in lipid packing, as quantified by GP, from  $0.128 \pm 0.006$  to  $0.392 \pm 0.003$  with Chol increasing in an approximate linearly fashion (Fig. 3C).

Increasing membrane lipid-packing also resulted in a concomitant slowdown of membrane lipid mobility (Fig. S3). To rule out that the reduction of the Fab diffusion coefficient with increasing lipid-packing was due to individual lipid deceleration, we compared the Fab diffusion and the diffusion of a fluorescently tagged lipid (DOPE-STAR RED at 1:1000 mole fraction) in otherwise same-composition GUVs (Fig. S3). At low Chol content (20%) the diffusion coefficient of the Fab is higher than that of individual lipids ( $8.3 \pm 0.7$  and  $5.9 \pm 0.6 \mu\text{m}^2\text{s}^{-1}$ , respectively) whereas, at high Chol content (50%), the Fab and the lipids diffuse at similar rate ( $4.1 \pm 0.3$  and  $4.2 \pm 0.5 \mu\text{m}^2\text{s}^{-1}$ , respectively). The reduction rate of the Fab diffusion coefficient with increasing Chol content is, therefore, much more pronounced than that of the lipids, supporting that Fab slowdown with increasing Chol is not due to individual lipid deceleration, but the result of a change in a collective biophysical property such as lipid-packing.

#### **4E10 Fab diffusion regime supports a non-specific electrostatic interaction with anionic membranes**

sFCS experiments of 4E10 Fab on virus-like vesicles had shown that the increase of the overall bilayer charge through an increase of PS content triggered a significant reduction of the 4E10 Fab diffusion coefficient (Fig. 2E). The negatively charged lipid PS is exposed on the viral membrane external leaflet (8, 46) and accounts for nearly 10% of the total HIV lipid content (18, 47). PS is, therefore, the major contributor to the envelope net charge. For this reason, we set to get further insight into the Fab electrostatic association to the HIV lipid-envelope. We studied the 4E10 Fab diffusion on a series of model PS:Chol:PC GUVs with increasing content of PS while keeping Chol content constant.

Increasing PS had the effect of increasing the vesicle overall negative charge and, in turn, the membrane surface potential ( $\psi_s$ ).  $\psi_s$  was calculated to be -40 mV for 15% PS and increased, in the negative sense, to -86 mV for 45% PS (Fig. 4A, inset). 4E10 Fab diffusion significantly decreased with increasing PS content, from  $12.2 \pm 0.8 \mu\text{m}^2 \text{s}^{-1}$  for the 15% PS mixture to  $5.5 \pm 0.4$

$\mu\text{m}^2\text{s}^{-1}$  for the 45% PS mixture (Fig. 4A-B). In contrast, the diffusion of individual lipids within the bilayer, which is essentially dependent on membrane lipid-packing, was not affected by  $\psi_s$ , averaging to  $4.8\pm0.2\ \mu\text{m}^2\text{s}^{-1}$  at 35% Chol irrespective of PS content (Fig. 4C).

4E10 Fab electrostatic association with a PS-containing membrane may either involve specific molecular recognition of PS polar-head or non-specific charge-driven interactions established through the Fab basic-residue containing MAPA surface (Fig. 1B). To address this question, we first tested sFCS capability to tell the different nature of the lipid-protein electrostatic association comparing the diffusion of 4E10 Fab to that of Annexin A5 at PS:Chol:PC vesicles of the same composition. Annexin A5 is a peripheral protein known to specifically dock onto single PS headgroups with high affinity ( $K_d\approx 20\text{ nM}$  (48)). Previous studies on supported bilayers using FRAP (Fluorescence Recovery After Photobleaching) and single-particle tracking have shown that proteins tightly bound to a single lipid in the bilayer diffuse at the same rate as the free lipid since the main component of the frictional drag is the viscosity of the bilayer through the lipid they are attached to (49, 50). Consequently, the diffusion coefficient of proteins bound to individual lipids does not depend on the relative concentration of the specific lipid ligands. On the other hand, proteins associated to the bilayer through less specific electrostatic interactions are expected to diffuse faster than individual lipids in the bilayer and to display dependence on the fraction of anionic lipids (51).

Annexin A5 diffusion was strikingly different to 4E10 Fab diffusional behaviour. Whereas the Fab diffusion slowed down with increasing PS molar fraction and, as a consequence, membrane surface potential (Fig. 4A-B), Annexin diffusion coefficient was not dependent on  $\psi_s$ , averaging to  $3.2\pm0.2\ \mu\text{m}^2\text{s}^{-1}$  (Fig. 4D). This behaviour is analogous to that of individual lipids (Fig. 4C), reflecting that Annexin A5 tightly binds to PS molecules diffusing along with them. Taking into account that Annexin A5 can self-assemble in 2D trimeric-arrays (52), the diffusion coefficient we have obtained is likely to be an average of individual and trimeric Annexin repeats



(associating to one and three PS copies, respectively), and, as a result, slightly lower than that observed for individual lipids.

This experiment comparing 4E10 and Annexin A5 diffusional behaviours reflected the potential of sFCS measurements to discern the nature of protein-lipid interactions. Thus, the results demonstrated that the membrane-bound 4E10 Fab does not dock onto individual PS molecules diffusing along with them, but, rather, slides over the bilayer surface, presumably subject to intermittent adsorption events due to non-specific charge-driven attractive forces.

To further confirm this result we studied the diffusional behaviour of 4E10 at anionic membranes with fixed PS content while increasing the buffer ionic strength (Fig. S4) (53). Increasing the ionic strength increases the electrolyte concentration, decreasing, in turn, vesicles  $\psi_s$  (Fig. S4, inset). Since membrane lipid mobility is largely unaffected by buffer ionic strength, a protein associated through a stereospecific interaction to the head-group of a lipid would diffuse at the same rate irrespective of the electrolyte concentration. We observed, however, that 4E10 diffused faster with increasing ionic strength (Fig. S4), reflecting that the electrostatic attraction between the anionic membrane and the Fab is more effectively screened by the growing number of electrolyte ions surrounding the Fab. This supported that the electrostatic contribution to Fab association with the bilayer is governed by a non-specific charge-driven interaction with the anionic membrane.

### **HCDR3 tryptophan residues and a group of basic residues orient 4E10 paratope on the membrane surface**

To acquire atomistic insight into the orientation and interactions of 4E10 with the membrane, we ran MD simulations of the 4E10 Fab in the presence of a DOPS:Chol:DOPC (45:35:20) bilayer. We had observed that 4E10 Fab diffusion on this membrane was the slowest of the lipid mixtures experimentally studied, suggesting strong Ab-membrane interactions. During 750 ns the overall 4E10 Fab structure remained stable as well as that of individual H and L chains, and the Constant

(C) and Variable (V) domains (Fig. 5A). This was further confirmed by clustering analysis of the 4E10 Fab coordinates, which showed only two rather similar 4E10 Fab conformations (Fig. S5A), indicating that the structural integrity of the 4E10 Fab was preserved. During the simulation, the HCDR3 loop only sampled a stable conformation (Fig. 5A and Fig. S5B). The HCDR3 loop maintained a specific 3D arrangement, characterized by having the W100 and W100b residues exposed (Fig. S5B) and prone to membrane insertion. Consistent with such disposition, the 4E10 Fab readily approached the membrane at the beginning of the simulation, inserting W100 and W100b into the bilayer and remaining anchored to the membrane for the rest of the simulation (Fig. 5B). The conservation of the HCDR3 conformation and its insertion into the lipid bilayer membrane correlated with the stabilization of a specific orientation of the H-chain-V-domain, which enables the MAPA patch to associate with the membrane surface (Fig. 5C). Overall, during the simulation the MPER binding pocket retained an orientation that would allow Fab docking onto Env on the viral membrane surface (compare Fig. 1A to 5D).

Further analysis of the interactions between the V-domain residues and the membrane lipids identified different types of contacts with varying probability (Fig. S6). A summary is shown in Fig. 5E, where V-domain residues with a high probability of interaction with PC, PS and Chol have been highlighted. In line with previous crystallographic studies (10), these results confirmed high probability contacts between phospholipids PC/PS and Fab residues W100/W100b and S25/G26/G27/S28/F29/S30, from the HCDR3 and HCDR1, respectively. In addition, they also allowed the identification of a group of basic residues, which have a high probability of interaction with PS molecules (K100E, R54, R77, R73, K23, R45, and R61) and cooperate with W100 and W100b to stabilise the Fab orientation (Fig. 5E and S6). Notably, Chol interacts with the HCDR3 apex residues W100/G100a/W100b (Figs. 5D,E).

To provide further robustness to the MD simulation results, an independent 250 ns simulation (MD replica II) was carried out, starting from the same system configuration as that

used for the original 750 ns simulation (MD replica I). The results obtained are in full agreement with those from MD replica I (Fig. S7 and S8).

## Discussion

Identification and characterisation of Ab-pathogen interactions is critical for vaccine design and therapy. A relatively new concept has been introduced in this area upon the discovery of anti-MPER Abs against HIV: the establishment of Ab-membrane interactions for effective engagement with antigens. The case of the anti-HIV 4E10 bnAb is paradigmatic in this sense since Ab-lipid interactions are essential for its neutralising activity (6, 7, 9). For this reason, determining the degree of specificity of Ab-lipid interactions in a membrane context has relevant and crucial functional consequences for vaccine design.

Among anti-MPER bnAbs, 4E10 shows the strongest membrane partitioning capacity. MPER recognition by 4E10 is thought to be favoured by the interplay of the hydrophobic residues W100 and W100b at the Ab HCDR3 with the membrane and its epitope (7, 9, 12). Besides, 4E10 has been shown to partition to PS-containing vesicles with the same lipid composition as used in this work ( $K_x = 0.6 \times 10^{-6}$  M) (7) and to weakly bind phospholipids immobilized on ELISA plates, including PS, PE, PA (phosphatidic acid) PG (phosphatidylglycerol) and PI (phosphatidylinositol) (54). This observation prompted subsequent crystallographic analyses of Fab 4E10 in complex with water-soluble, short-acyl chain derivatives of those phospholipids (10). Upon crystallization, Fab residues from the HCDR1 and HCDR3 were indeed found establishing interactions with glycerophosphate moieties, supporting the accommodation of phospholipid interfacial groups onto the MAPA during the process of antigen binding. However, whether 4E10 specifically binds all or some of these lipids in a membrane context, and how the process may contribute to Ab-MPER binding is unclear.

One suitable methodology to estimate the contribution of specific lipids to protein-protein interactions that evolve in the membrane interface environment is the study of proteins

diffusional regime. Diffusion of soluble proteins in solution is dependent on their hydrodynamic radius, solvent temperature and viscosity. In contrast, lateral translation of molecules fully embedded in a membrane is weakly dependent on their radius, but strongly dependent on the bilayer thickness (55, 56), in turn primarily determined by lipid packing. Peripheral proteins represent an intermediate scenario since they cannot freely diffuse, but they are not deeply embedded in the membrane either. They are, instead, associated to the bilayer in a shallow position through attractive electrostatic forces and/or hydrophobic anchoring (Fig. 1B). Each of these interactions contributes to the protein frictional drag at the membrane in an additive fashion (50, 57), defining the protein diffusion rate, and therefore allowing the investigation of the nature of protein-lipid contacts.

Our results, based on sFCS diffusion measurements, demonstrate that long-range electrostatic and hydrophobic interactions cooperate to promote 4E10 association to the membrane (Fig. 2A-B). We found that both interactions slow down 4E10 Fab dynamics at the membrane (Fig. 2D-E). Diffusion experiments of the Fab on model membranes with increasing cholesterol (Fig. 3) or PS content (Fig. 4) show an inverse relationship between the concentration of these lipids and 4E10 Fab diffusivity, suggesting that hydrophobic and electrostatic interactions sustain insertion of the Ab in the membrane. Since the intercalation of hydrophobic residues in the bilayer contributes to total friction (57), 4E10 Fab slowdown at the membrane with increasing lipid packing (Fig. 3A) due to increased Chol content is consistent with 4E10 Fab hydrophobic anchoring at the membrane.

The non-specific nature of the electrostatic interaction of 4E10 with the membrane was supported by the different diffusion patterns on PS:Chol:PC bilayers of the 4E10 Fab and those of a protein known to bind PS in a lipid-specific manner (Annexin A5) (Fig. 4). Dependence of membrane diffusion rates on surface potential (through a change of PS mole fraction and ionic strength) ruled out the existence of stereospecific binding of this anionic phospholipid to 4E10.

Increased surface potential may both cause an increase in the frequency of protein adsorption events or a stronger, deeper protein binding in the membrane. While both effects would result in the slowdown of a protein, a deeper 4E10 Fab insertion in the bilayer (through HCDR3 W100 and W100b residues) is not expected to be altered by surface charge density, since tryptophan residues accommodate in the vicinity of the phospholipid glycerol groups (58). For this reason, although we cannot fully rule out that surface charge affected 4E10 hydrophobic association, we expect this to be of small or unappreciable effect.

This conclusion, drawn from diffusion sFCS experiments, was further supported by MD simulations (Fig. 5). In line with previous crystallographic work (10), MD simulations of the Fab at then membrane suggest high probability contacts between PC/PS and residues from HCDR1 and HCDR3 (Fig. 5E and S6), that would be responsible for 4E10 hydrophobic association to the membrane. Moreover, PS high probability contacts with the Fab involved several basic residues (Fig. 5E and Table S1), suggesting a non-specific charge-driven attraction between the negatively charged PS and the basic residues on the protein surface. This conclusion is also consistent with previous vesicle binding experiments performed by our group (7) and others (45).

Our MD simulations also showed that the aromatic HCDR3 residues W100 and W100b, which were associated to lipid tails in Fab-phospholipid co-crystals (10), can favourably stack with Chol. Interestingly, acyl-chain interactions seem to be accompanied by a conformational change that reorients the HCDR3 loop (10). This raises the possibility of loop conformations stabilised in the membrane through interaction with different lipid species and/or MPER helix.

Altogether, we envision a multiple-lipid interaction model where all phospholipid molecules in the viral membrane interact intermittently, but favourably, with the lipid-binding sub-sites on 4E10 MAPA, anionic PS molecules establish additional electrostatic interactions with positively charged residues, and sterol rings and phospholipid acyl chains alternate occupancy of the membrane integral groove in between W100 and W100b rings.

## Conclusions

We have investigated 4E10-membrane interaction studying the diffusion regime of 4E10 Fab at the bilayer and correlating it to the collective membrane biophysical properties lipid-packing and membrane surface potential. MD simulations have provided further insight into the 4E10-membrane interaction. Our experiments provide unprecedented and rigorous information about the dynamics of the Ab in a virus-like membrane environment.

Our data support that, since 4E10 does not spontaneously bind to the virus membrane in the absence of the viral protein Env (8), non-specific electrostatic Ab-lipid interactions increase 4E10 affinity for Env by providing extra contact sites on the viral surface, enlarging the interacting area, and/or facilitating the insertion of the Ab in the membrane after MPER engagement, thus, stabilising the 4E10-Env complex. The orientation of the 4E10 Fab at the membrane as observed during MD simulations reinforces this idea. We anticipate that these results will help in the design of the next generation of MPER-based immunogens.

## Acknowledgements

Supported by Ministerio de Economía y Competitividad in Spain grants (BIO2015-64221-R (MINECO/AEI/FEDER UE) and RTI2018-095624-B-C21 (MINECO/AEI/FEDER UE) to JLN and BFU2015-65625-P (MINECO/FEDER UE)), Basque Government grant IT1196-19, and doctoral studentship to PC and ER, and a FPU doctoral scholar ship to AGV (FPU2016-01727). PC also acknowledges a research associate contract at the University of the Basque Country (DOCREC18/01) and a postdoctoral fellowship from the Basque Government (POS\_2018\_1\_0066). LD acknowledges ANII and IPMon for funding his post-doctoral fellowship. The computational work was partly performed under a RES (Red Española de Supercomputación) award. In particular, CD gratefully acknowledges the computer resources at Magerit (Madrid) and technical support provided by the IT team. JRI acknowledges the use of

computational resources from CESGA (Centro de Supercomputación de Galicia). We gratefully thank Unai Lorenzo-Sierra for developing sFCS software and analysis algorithms.

### **Author contributions**

PC performed experiments, and contributed to the experimental design, discussion and paper writing; LD performed the MD simulations; IROA performed experiments; ER produced antibodies and designed the labelling strategy; AGV performed experiments; GH-M set sFCS methodology up; CD supervised the MD simulations and contributed to the discussion; JL Nieva formulated the experiment and contributed to the discussion and paper writing; JRI supervised the experimental design and contributed to the discussion and paper writing.

## Figures

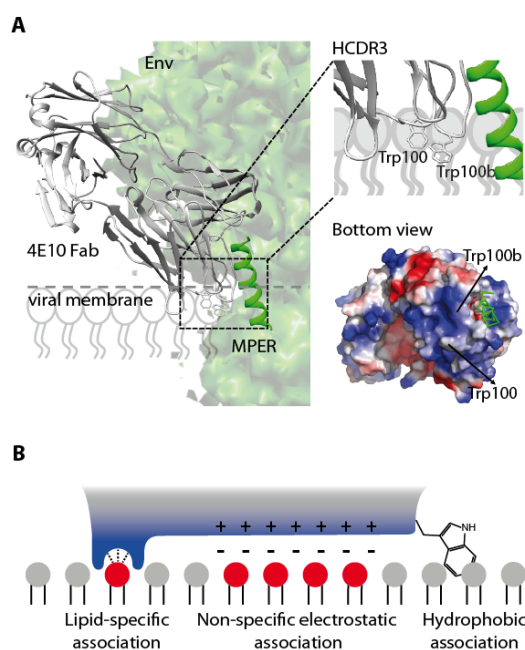


**Figure 1. Lipid contribution to 4E10 recognition of HIV Env. (A)** Presumed interacting geometry of 4E10 Fab (grey) with the Env glycoprotein (light green) MPER region (residues 671-693, dark green) and the HIV membrane. This model is based on the PDB IDs 4XBG for 4E10 and 2MG2 for MPER. Env glycoprotein trimer contour has been adapted from the cryo-electron microscopy structure with EMDB accession number EMD-3308. The grey dotted line indicates the approximate level of the membrane interface. Fab hydrophobic sites W100 and W100b at the HCDR3 loop (top inset) and cationic patches (in blue, bottom inset) are known to be involved in gp41 recognition. **(B)** Cartoon illustrating the different antibody-membrane interaction modes interrogated in this work. From left to right: lipid-specific interaction, represented by a prominent positive lobe and a network of stereospecific hydrogen-bonding interactions that bind the protein to a single lipid copy; non-specific charge-driven attraction through poly-cationic patches at the protein surface, and hydrophobic protein-membrane association. Red indicates anionic lipid species.



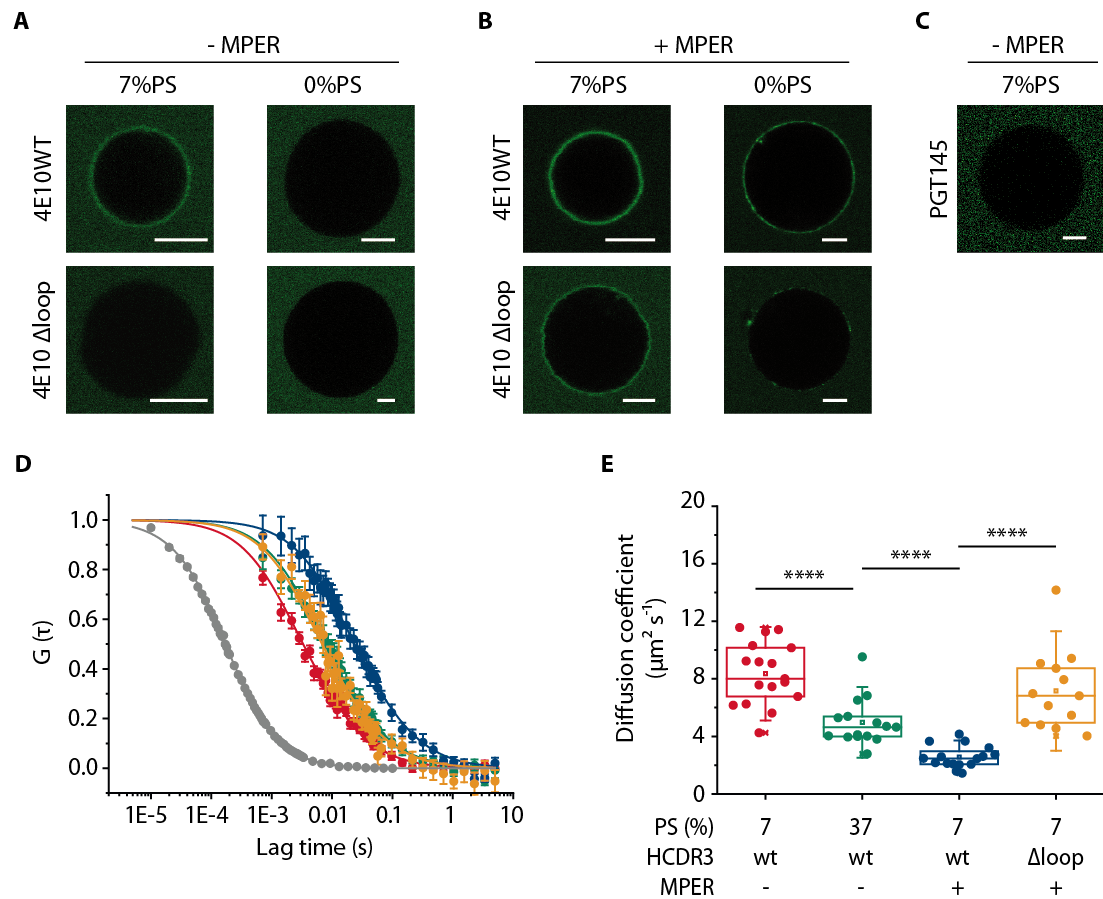


**Figure 2. Electrostatic and hydrophobic interactions play a critical role in efficient lipid-mediated antigen binding:** **(A)** Association of the 4E10 Fab to the virus-like negatively charged membrane at physiological ionic strength. A neutral surface or deletion of the hydrophobic residues at 4E10 Fab HCDR3 thwarted the association. **(B)** 4E10 antigen (MPER peptide) markedly enhances Fab binding to the vesicle-antigen ensemble. In the presence of MPER, electrostatic and hydrophobic interactions between the lipid and the 4E10 Fab promote binding to the vesicle-antigen system. **(C)** The bnAb PGT145 does not associate to the viral-like membranes, confirming the non-random association of 4E10. **(D)** Representative correlation curves of 4E10 Fab in solution (grey) and the membrane of virus-like GU (colours as in E). *Curves were normalised to their value at  $G(0)$  after fitting for easier comparison.* **(E)** The diffusion of the 4E10 Fab on the virus-like vesicle is slowed down by its interaction with the negatively-charged lipids at the membrane, the MPER peptide loaded on the membrane and the 4E10 Fab HCDR3 loop. A-B: Scale bar is 4  $\mu\text{m}$ . E: Whiskers indicate  $\pm 1.5 \times \text{SD}$ .

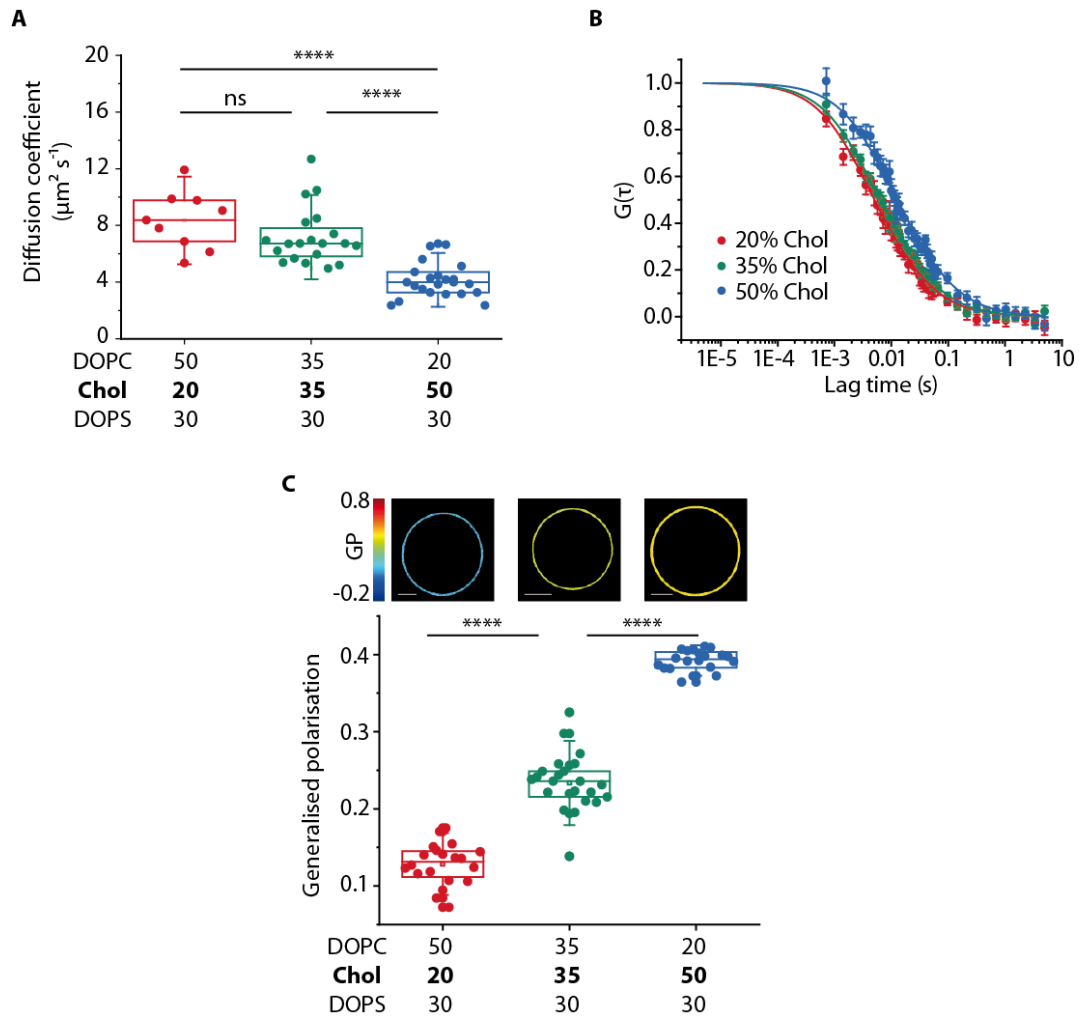


**Figure 3. Cholesterol content modulates 4E10 Fab binding to the membrane. (A)** 4E10 Fab diffusion at the membrane is slowed down when Chol content in the membrane increases. **(B)** Representative correlation curves of 4E10 Fab diffusing on the vesicles in (A). **(C)** Cholesterol content in the membrane has a direct effect in lipid packing, quantified by GP measurements. Top, representative false-colour GP images of the GUVs used to quantify lipid packing. A-C: Whiskers indicate  $\pm 1.5 \times \text{SD}$ . C: Scale bar is  $5 \mu\text{m}$  in all cases.

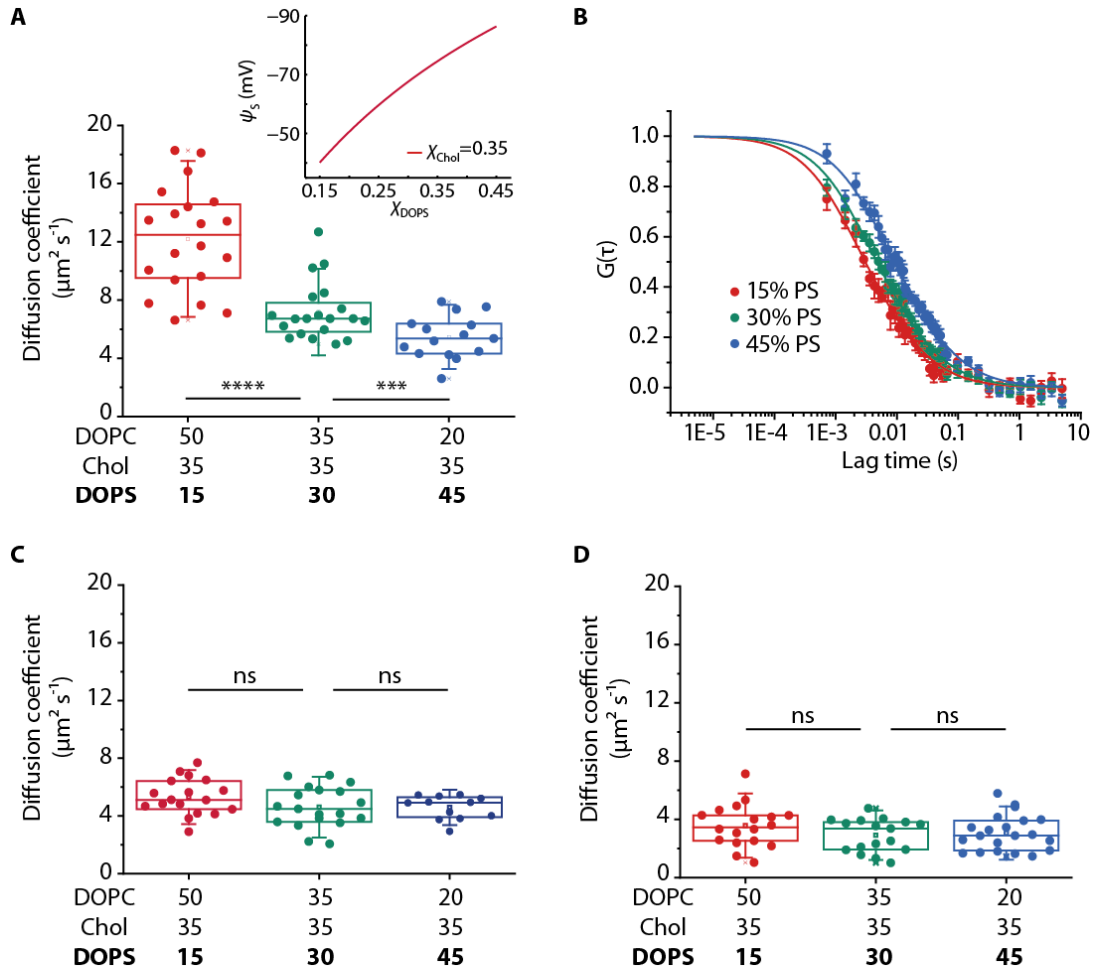


**Figure 4. 4E10 Fab binding to the membrane is driven by negative charges. (A)** 4E10 Fab diffusion at the membrane is significantly slowed down with increasing PS content. Inset: Membrane surface potential with increasing PS content at physiological ionic strength (150 nM). **(B)** Representative correlation traces of the Fab diffusing in (A). **(C).** Diffusion of a DOPE-Star Red molecule (1:1000 mole fraction) in the DOPS:Chol:DOPC mixture does not change with increasing PS content. **(D)** The diffusion of Annexin A5 on a charged bilayer in the presence of  $\text{Ca}^{2+}$  is not dependent on the membrane surface potential and is consistent with individual lipid diffusion shown in (C). Whiskers indicate  $\pm 1.5 \times \text{SD}$  in all cases.

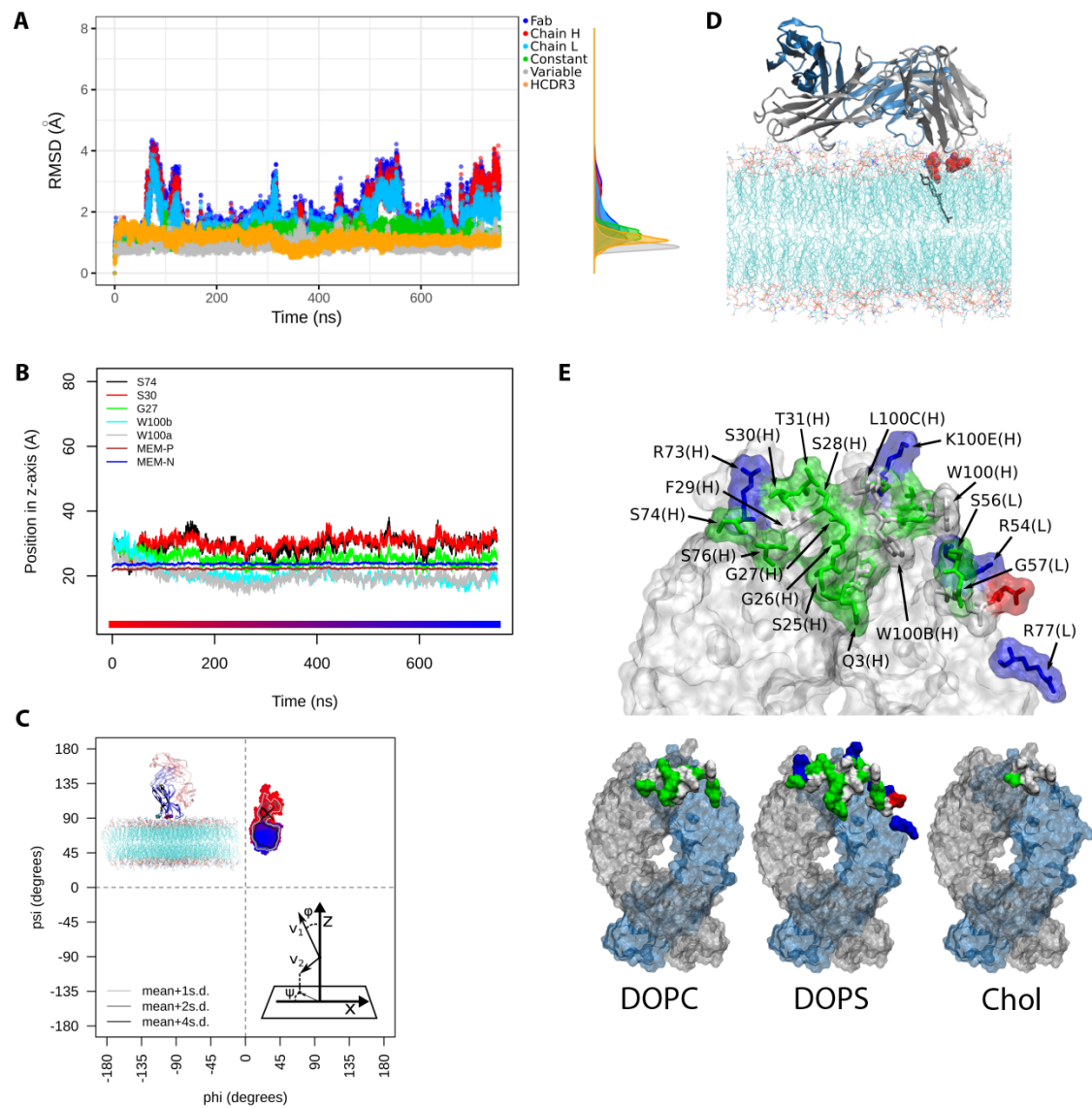


**Figure 5. Atomistic insight into 4E10-membrane interactions (MD replica I: 750 ns).** **(A)**  $\alpha$ -RMSD (Root Mean Square Deviation) of the complete 4E10 Fab, heavy (H) and light (L) chains, constant domain, variable domain, and the HCDR3 loop, measured during the MD simulation. Flexible loops were not considered in the RMSD measurement except for HCDR3. **(B)** z-axis position of P and N lipid atoms in the membrane leaflet closer to 4E10 Fab, and of the geometric centre of protein residues S74, S30, G27, W100 and W100b. The bottom colour bar matches the simulation time points in panel (C). **(C)** Sampling of the  $\phi/\psi$  space of the 4E10 Fab during the MD simulation. Dots colour indicates the time as in (B): red, shorter simulation times; blue, longer times.  $\phi$  corresponds to the angle between the protein first principal axis

(v1) and the simulation box z axis (normal to the membrane), and  $\psi$  corresponds to the angle between the second principal axis (v2) of the protein and the x axis of the simulation box (see bottom right inset in panel C). Isodensity contour lines are shown to display density values: mean+1sd (light grey), mean+2sd (grey) and, mean+4sd (dark grey). The black cross indicates the orientation of the starting configuration, illustrated in the top-left inset. **(D)** Representative structure taken from the high density region of the  $\phi/\psi$  space. A cholesterol molecule is shown interacting with residues W100 and W100b. **(E)** Top: 4E10 Fab residues with high probability of contact (setting 5 Å as the cut-off distance between any lipid heavy atom and any protein heavy atom) with the membrane are indicated (basic: blue; acidic: red; polar: green; hydrophobic: white). Bottom: same as in the top panel but discriminating according to the specific lipid in contact with the protein (see Figure S6 for the corresponding probability of contact distributions). The 4E10 Fab surface is coloured by chain (H: grey, L: blue).

## References

1. Burton, D. R., and L. Hangartner. 2016. Broadly Neutralizing Antibodies to HIV and Their Role in Vaccine Design. In *Annual Review of Immunology*. Annual Review of Immunology, Vol 34. D. R. Littman and W. M. Yokoyama, editors, pp. 635-659.
2. Brunel, F. M., M. B. Zwick, R. M. F. Cardoso, J. D. Nelson, I. A. Wilson, D. R. Burton, and P. E. Dawson. 2006. Structure-function analysis of the epitope for 4E10, a broadly neutralizing human immunodeficiency virus type 1 antibody. *Journal of Virology* 80(4):1680-1687.
3. Cardoso, R. M. F., M. B. Zwick, R. L. Stanfield, R. Kunert, J. M. Binley, H. Katinger, D. R. Burton, and I. A. Wilson. 2005. Broadly neutralizing anti-HIV antibody 4E10 recognizes a helical conformation of a highly conserved fusion-associated motif in gp41. *Immunity* 22(2):163-173.
4. Vishwanathan, S. A., and E. Hunter. 2008. Importance of the membrane-perturbing properties of the membrane-proximal external region of human immunodeficiency virus type 1 gp41 to viral fusion. *Journal of Virology* 82(11):5118-5126.
5. Suarez, T., W. R. Gallaher, A. Agirre, F. M. Goni, and J. L. Nieva. 2000. Membrane interface-interacting sequences within the ectodomain of the human immunodeficiency virus type 1 envelope glycoprotein: Putative role during viral fusion. *Journal of Virology* 74(17):8038-8047.
6. Alam, S. M., M. Morelli, S. M. Dennison, H. X. Liao, R. J. Zhang, S. M. Xia, S. Rits-Volloch, L. Sun, S. C. Harrison, B. F. Haynes, and B. Chen. 2009. Role of HIV membrane in neutralization by two broadly neutralizing antibodies. *Proc. Natl. Acad. Sci. U. S. A.* 106(48):20234-20239.
7. Rujas, E., J. M. M. Caaveiro, S. Insausti, M. Garca-Porras, K. Tsumoto, and J. L. Nieva. 2017. Peripheral Membrane Interactions Boost the Engagement by an Anti-HIV-1 Broadly Neutralizing Antibody. *J. Biol. Chem.* 292(13):5571-5583.
8. Carravilla, P., J. Chojnacki, E. Rujas, S. Insausti, E. Largo, D. Waithe, B. Apellaniz, T. Sicard, J.-P. Julien, C. Eggeling, and J. L. Nieva. 2019. Molecular recognition of the native HIV-1 MPER revealed by STED microscopy of single virions. *Nat. Commun.* 10.
9. Scherer, E. M., D. P. Leaman, M. B. Zwick, A. J. McMichael, and D. R. Burton. 2010. Aromatic residues at the edge of the antibody combining site facilitate viral glycoprotein recognition through membrane interactions. *Proc. Natl. Acad. Sci. U. S. A.* 107(4):1529-1534.
10. Irimia, A., A. Sarkar, R. L. Stanfield, and I. A. Wilson. 2016. Crystallographic Identification of Lipid as an Integral Component of the Epitope of HIV Broadly Neutralizing Antibody 4E10. *Immunity* 44(1):21-31.
11. Irimia, A., A. M. Serra, A. Sarkar, R. Jacak, O. Kalyuzhniy, D. Sok, K. L. Saye-Francisco, T. Schiffner, R. Tingle, M. Kubitz, Y. Adachi, R. L. Stanfield, M. C. Deller, D. R. Burton, W. R. Schief, and I. A. Wilson. 2017. Lipid interactions and angle of approach to the HIV-1 viral membrane of broadly neutralizing antibody 10E8: Insights for vaccine and therapeutic design. *PLoS Pathog.* 13(2).
12. Rujas, E., S. Insausti, M. Garcia-Porras, R. Sanchez-Eugenia, K. Tsumoto, J. L. Nieva, and J. M. M. Caaveiro. 2017. Functional Contacts between MPER and the Anti-HIV-1 Broadly Neutralizing Antibody 4E10 Extend into the Core of the Membrane. *Journal of Molecular Biology* 429(8):1213-1226.
13. Rujas, E., N. Gulzar, K. Morante, K. Tsumoto, J. K. Scott, J. L. Nieva, and J. M. M. Caaveiro. 2015. Structural and Thermodynamic Basis of Epitope Binding by Neutralizing and Nonneutralizing Forms of the Anti-HIV-1 Antibody 4E10. *Journal of Virology* 89(23):11975-11989.

14. Ries, J., and P. Schwille. 2006. Studying slow membrane dynamics with continuous wave scanning fluorescence correlation spectroscopy. *Biophys. J.* 91(5):1915-1924.
15. Heinemann, F., V. Betaneli, F. A. Thomas, and P. Schwille. 2012. Quantifying Lipid Diffusion by Fluorescence Correlation Spectroscopy: A Critical Treatise. *Langmuir* 28(37):13395-13404. Article.
16. Huarte, N., P. Carravilla, A. Cruz, M. Lorzate, J. A. Nieto-Garai, H.-G. Kraeusslich, J. Perez-Gil, J. Requejo-Isidro, and J. L. Nieva. 2016. Functional organization of the HIV lipid envelope. *Sci Rep* 6:34190.
17. Carravilla, P., J. L. Nieva, F. M. Goni, J. Requejo-Isidro, and N. Huarte. 2015. Two-Photon Laurdan Studies of the Ternary Lipid Mixture DOPC:SM:Cholesterol Reveal a Single Liquid Phase at Sphingomyelin:Cholesterol Ratios Lower Than 1. *Langmuir* 31(9):2808-2817.
18. Brugger, B., B. Glass, P. Haberkant, I. Leibrecht, F. T. Wieland, and H. G. Krausslich. 2006. The HIV lipidome: A raft with an unusual composition. *Proc. Natl. Acad. Sci. U. S. A.* 103(8):2641-2646.
19. Shnyrova, A. V., P. V. Bashkirov, S. A. Akimov, T. J. Pucadyil, J. Zimmerberg, S. L. Schmid, and V. A. Frolov. 2013. Geometric Catalysis of Membrane Fission Driven by Flexible Dynamin Rings. *Science* 339(6126):1433-1436.
20. Parasassi, T., G. De Stasio, G. Ravagnan, R. M. Rusch, and E. Gratton. 1991. QUANTITATION OF LIPID PHASES IN PHOSPHOLIPID-VESICLES BY THE GENERALIZED POLARIZATION OF LAURDAN FLUORESCENCE. *Biophys. J.* 60(1):179-189.
21. Gaus, K., T. Zech, and T. Harder. 2006. Visualizing membrane microdomains by Laurdan 2-photon microscopy. *Molecular Membrane Biology* 23(1):41-48.
22. de Las Heras-Martinez, G., J. Andrieu, B. Larijani, and J. Requejo-Isidro. 2018. Quantifying intracellular equilibrium dissociation constants using single-channel time-resolved FRET. *J. Biophotonics* 11(1):e201600272.
23. Andelman, D. 2006. Introduction to Electrostatics in Soft and Biological Matter. *Soft condensed matter physics in molecular and cell biology*. W. Poon and D. Andelman, editors. Taylor & Francis, pp. 97-122.
24. Anandakrishnan, R., B. Aguilar, and A. V. Onufriev. 2012. H++3.0: automating pK prediction and the preparation of biomolecular structures for atomistic molecular modeling and simulations. *Nucleic Acids Research* 40(W1):W537-W541.
25. Myers, J., G. Grothaus, S. Narayanan, and A. Onufriev. 2006. A simple clustering algorithm can be accurate enough for use in calculations of pKs in macromolecules. *Proteins-Structure Function and Bioinformatics* 63(4):928-938.
26. Gordon, J. C., J. B. Myers, T. Foltá, V. Shoja, L. S. Heath, and A. Onufriev. 2005. H++: a server for estimating pK(a)s and adding missing hydrogens to macromolecules. *Nucleic Acids Research* 33:W368-W371.
27. Jo, S., T. Kim, V. G. Iyer, and W. Im. 2008. Software news and updates - CHARMM-GUI: A web-based graphical user interface for CHARMM. *Journal of Computational Chemistry* 29(11):1859-1865.
28. Lee, J., X. Cheng, J. M. Swails, M. S. Yeom, P. K. Eastman, J. A. Lemkul, S. Wei, J. Buckner, J. C. Jeong, Y. Qi, S. Jo, V. S. Pande, D. A. Case, C. L. Brooks, III, A. D. MacKerell, Jr., J. B. Klauda, and W. Im. 2016. CHARMM-GUI Input Generator for NAMD, GROMACS, AMBER, OpenMM, and CHARMM/OpenMM Simulations Using the CHARMM36 Additive Force Field. *Journal of Chemical Theory and Computation* 12(1):405-413.
29. Wu, E. L., X. Cheng, S. Jo, H. Rui, K. C. Song, E. M. Davila-Contreras, Y. Qi, J. Lee, V. Monje-Galvan, R. M. Venable, J. B. Klauda, and W. Im. 2014. CHARMM-GUI Membrane Builder Toward Realistic Biological Membrane Simulations. *Journal of Computational Chemistry* 35(27):1997-2004.
30. Jo, S., J. B. Lim, J. B. Klauda, and W. Im. 2009. CHARMM-GUI Membrane Builder for Mixed Bilayers and Its Application to Yeast Membranes. *Biophys. J.* 97(1):50-58.

31. Jo, S., T. Kim, and W. Im. 2007. Automated Builder and Database of Protein/Membrane Complexes for Molecular Dynamics Simulations. *PLoS One* 2(9).
32. Huang, J., S. Rauscher, G. Nawrocki, T. Ran, M. Feig, B. L. de Groot, H. Grubmuller, and A. D. MacKerell. 2017. CHARMM36m: an improved force field for folded and intrinsically disordered proteins. *Nat. Methods* 14(1):71-73.
33. Klauda, J. B., R. M. Venable, J. A. Freites, J. W. O'Connor, D. J. Tobias, C. Mondragon-Ramirez, I. Vorobyov, A. D. MacKerell, and R. W. Pastor. 2010. Update of the CHARMM All-Atom Additive Force Field for Lipids: Validation on Six Lipid Types. *J. Phys. Chem. B* 114(23):7830-7843.
34. Jorgensen, W. L., J. Chandrasekhar, J. D. Madura, R. W. Impey, and M. L. Klein. 1983. COMPARISON OF SIMPLE POTENTIAL FUNCTIONS FOR SIMULATING LIQUID WATER. *Journal of Chemical Physics* 79(2):926-935.
35. Beglov, D., and B. Roux. 1994. FINITE REPRESENTATION OF AN INFINITE BULK SYSTEM - SOLVENT BOUNDARY POTENTIAL FOR COMPUTER-SIMULATIONS. *Journal of Chemical Physics* 100(12):9050-9063.
36. Luo, Y., and B. Roux. 2010. Simulation of Osmotic Pressure in Concentrated Aqueous Salt Solutions. *Journal of Physical Chemistry Letters* 1(1):183-189.
37. Feller, S. E., Y. H. Zhang, R. W. Pastor, and B. R. Brooks. 1995. CONSTANT-PRESSURE MOLECULAR-DYNAMICS SIMULATION - THE LANGEVIN PISTON METHOD. *Journal of Chemical Physics* 103(11):4613-4621.
38. Martyna, G. J., D. J. Tobias, and M. L. Klein. 1994. CONSTANT-PRESSURE MOLECULAR-DYNAMICS ALGORITHMS. *Journal of Chemical Physics* 101(5):4177-4189.
39. Izaguirre, J. A., D. P. Catarella, J. M. Wozniak, and R. D. Skeel. 2001. Langevin stabilization of molecular dynamics. *Journal of Chemical Physics* 114(5):2090-2098.
40. Essmann, U., L. Perera, M. L. Berkowitz, T. Darden, H. Lee, and L. G. Pedersen. 1995. A SMOOTH PARTICLE MESH EWALD METHOD. *Journal of Chemical Physics* 103(19):8577-8593.
41. Tuckerman, M., B. J. Berne, and G. J. Martyna. 1992. REVERSIBLE MULTIPLE TIME SCALE MOLECULAR-DYNAMICS. *Journal of Chemical Physics* 97(3):1990-2001.
42. Andersen, H. C. 1983. RATTLE - A VELOCITY VERSION OF THE SHAKE ALGORITHM FOR MOLECULAR-DYNAMICS CALCULATIONS. *Journal of Computational Physics* 52(1):24-34.
43. Phillips, J. C., R. Braun, W. Wang, J. Gumbart, E. Tajkhorshid, E. Villa, C. Chipot, R. D. Skeel, L. Kale, and K. Schulten. 2005. Scalable molecular dynamics with NAMD. *Journal of Computational Chemistry* 26(16):1781-1802.
44. Walker, L. M., M. Huber, K. J. Doores, E. Falkowska, R. Pejchal, J. P. Julien, S. K. Wang, A. Ramos, P. Y. Chan-Hui, M. Moyle, J. L. Mitcham, P. W. Hammond, O. A. Olsen, P. Phung, S. Fling, C. H. Wong, S. Phogat, T. Wrin, M. D. Simek, W. C. Koff, I. A. Wilson, D. R. Burton, P. Poignard, and G. P. I. Protocol. 2011. Broad neutralization coverage of HIV by multiple highly potent antibodies. *Nature* 477(7365):466-U117.
45. Finton, K. A. K., K. Larimore, H. B. Larman, D. Friend, C. Correnti, P. B. Rupert, S. J. Elledge, P. D. Greenberg, and R. K. Strong. 2013. Autoreactivity and Exceptional CDR Plasticity (but Not Unusual Polyspecificity) Hinder Elicitation of the Anti-HIV Antibody 4E10. *PLoS Pathog.* 9(9).
46. Callahan, M. K., P. M. Popernack, S. Tsutsui, L. Truong, R. A. Schlegel, and A. J. Henderson. 2003. Phosphatidylserine on HIV envelope is a cofactor for infection of monocytic cells. *Journal of Immunology* 170(9):4840-4845.
47. Chan, R., P. D. Uchil, J. Jin, G. Shui, D. E. Ott, W. Mothes, and M. R. Wenk. 2008. Retroviruses Human Immunodeficiency Virus and Murine Leukemia Virus Are Enriched in Phosphoinositides. *Journal of Virology* 82(22):11228-11238.
48. Raynal, P., and H. B. Pollard. 1994. ANNEXINS - THE PROBLEM OF ASSESSING THE BIOLOGICAL ROLE FOR A GENE FAMILY OF MULTIFUNCTIONAL CALCIUM-BINDING AND



- PHOSPHOLIPID-BINDING PROTEINS. *Biochimica Et Biophysica Acta-Reviews on Biomembranes* 1197(1):63-93.
49. Tamm, L. K. 1988. LATERAL DIFFUSION AND FLUORESCENCE MICROSCOPE STUDIES ON A MONOCLONAL-ANTIBODY SPECIFICALLY BOUND TO SUPPORTED PHOSPHOLIPID-BILAYERS. *Biochemistry* 27(5):1450-1457.
  50. Knight, J. D., M. G. Lerner, J. G. Marciano-Velazquez, R. W. Pastor, and J. J. Falke. 2010. Single Molecule Diffusion of Membrane-Bound Proteins: Window into Lipid Contacts and Bilayer Dynamics. *Biophys. J.* 99(9):2879-2887.
  51. Golebiewska, U., A. Gambhir, G. Hangyas-Mihalyne, I. Zaitseva, J. Radler, and S. McLaughlin. 2006. Membrane-bound basic peptides sequester multivalent (PIP<sub>2</sub>), but not monovalent (PS), acidic lipids. *Biophys. J.* 91(2):588-599.
  52. Gerke, V., C. E. Creutz, and S. E. Moss. 2005. Annexins: Linking Ca<sup>2+</sup> signalling to membrane dynamics. *Nat. Rev. Mol. Cell Biol.* 6(6):449-461.
  53. Shi, X., M. Kohram, X. Zhuang, and A. W. Smith. 2016. Interactions and Translational Dynamics of Phosphatidylinositol Bisphosphate (PIP<sub>2</sub>) Lipids in Asymmetric Lipid Bilayers. *Langmuir* 32(7):1732-1741.
  54. Matyas, G. R., Z. Beck, N. Karasawas, and C. R. Alving. 2009. Lipid binding properties of 4E10, 2175, and WR304 monoclonal antibodies that neutralize HIV-1. *Biochimica Et Biophysica Acta-Biomembranes* 1788(3):660-665.
  55. Saffman, P. G., and M. Delbruck. 1975. BROWNIAN-MOTION IN BIOLOGICAL-MEMBRANES. *Proc. Natl. Acad. Sci. U. S. A.* 72(8):3111-3113.
  56. Ramadurai, S., A. Holt, V. Krasnikov, G. van den Bogaart, J. A. Killian, and B. Poolman. 2009. Lateral Diffusion of Membrane Proteins. *J. Am. Chem. Soc.* 131(35):12650-12656.
  57. Ziemba, B. P., and J. J. Falke. 2013. Lateral diffusion of peripheral membrane proteins on supported lipid bilayers is controlled by the additive frictional drags of (1) bound lipids and (2) protein domains penetrating into the bilayer hydrocarbon core. *Chemistry and Physics of Lipids* 172:67-77.
  58. Yau, W. M., W. C. Wimley, K. Gawrisch, and S. H. White. 1998. The preference of tryptophan for membrane interfaces. *Biochemistry* 37(42):14713-14718.